Available online at www.sciencedirect.com

ScienceDirect

journal homepage: www.elsevier.com/locate/he

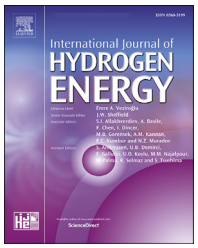

Performance of TiO_2 nanoparticles synthesized by microwave and solvothermal methods as photoanode in dye-sensitized solar cells (DSSC)

Venkatraman Madurai Ramakrishnan [a,b], *Selvakumar Pitchaiya* [a,b], *N. Muthukumarasamy* [a], *Kristin Kvamme* [c], *G. Rajesh* [d], *S. Agilan* [a], *Arivalagan Pugazhendhi* [e,*], *Dhayalan Velauthapillai* [b]

[a] *Department of Physics, Coimbatore Institute of Technology, Coimbatore - 641 014, Tamil Nadu, India*
[b] *Department of Engineering and Sciences, Western Norway University of Applied Sciences, Bergen, Norway*
[c] *Department of Safety, Chemistry and Biomedical Laboratory Sciences, Western Norway University of Applied Sciences, Bergen, Norway*
[d] *Department of Physics, University of Chile, Santiago, Chile*
[e] *Institute of Research and Development, Duy Tan University, Da Nang 550000, Viet Nam*

HIGHLIGHTS

- Comparison of the TiO_2 nanoparticles prepared by microwave and solvothermal methods.
- For the effective comparison, similar precursors were utilized in the synthesis.
- Structural, optical and morphological characteristics of the TiO_2 prepared by two methods.
- TiO_2 nanoparticles by microwave-assisted technique exhibited 7.44% efficiency.

ARTICLE INFO

Article history:
Received 4 March 2020
Received in revised form
12 June 2020
Accepted 2 July 2020
Available online 1 August 2020

Keywords:
TiO_2 nanoparticles
Solvothermal
Microwave
Photoanodes
Dye-sensitized solar cells

ABSTRACT

In this work, a direct comparison of the properties of the TiO_2 nanoparticles prepared by microwave and solvothermal methods were carried out and its performance as photoanode in dye-sensitized solar cells (DSSC) was analyzed. Though previously some works exist on the preparation of TiO_2 nanoparticles by solvothermal or microwave methods, they could not be compared directly as the experiment conditions such as choice of solvent, precursors and reaction temperatures were not virtually same. Herein, TiO_2 nanoparticles were synthesized by microwave and solvothermal methods using the same initial precursors and properties of the prepared nanoparticles were compared. From the X-ray diffraction pattern and Raman analysis, the prepared nanoparticles in both the cases were found to be of anatase phase. Optical properties and its carrier lifetime were studied using UV–Vis absorption, photoluminescence (PL) analysis and PL lifetime studies, respectively. Further, its morphology analyzed using scanning electron microscope (SEM) and transmission electron microscope (TEM) images, and SAED (selected area electron diffraction) patterns reveals the polycrystalline nature of the prepared nanoparticles. The surface area and the pore size distribution were studied using BET (Brunauer–Emmett–Teller) and BJH (Barrett–Joyner–Halenda) analysis, which revealed its mesoporous nature and uniform pore distribution. The chemical states of the prepared nanoparticles were further characterized using X-ray photoelectron spectroscopy. The DSSC was fabricated using the

* *Corresponding author.*
E-mail address: arivalaganpugazhendhi@duytan.edu.vn (A. Pugazhendhi).
https://doi.org/10.1016/j.ijhydene.2020.07.018

prepared TiO_2 nanoparticles as photoanodes. Further, the power conversion efficiency and the electron transport properties were analyzed.

Introduction

Light-induced electricity generation is one of the hot topics of research today. Among the current different solar cell technologies, third generation solar cell technologies such as dye-sensitized and perovskite solar cells exhibit promising candidature as a cost-effective alternative to conventional p–n junction solar cells [1–7]. Dye-sensitized solar cells (DSSC) work under the concept of photoelectrochemical process, where, conducting glass substrates coated with wide bandgap mesoporous nanocrystalline material sensitized using a monolayer of the dye is used as photoanode. The organic solvent containing iodide/triiodide redox couple system is used as an electrolyte, effective triiodide reduction catalyst such as platinum or carbon-based materials are preferred for the counter electrode [8–10].

As the vital processes such as light harvesting and charge transfer happen at the photoanode in DSSC [1], it has been extensively studied to improve the efficiency of the solar cells. Wide bandgap semiconductors are generally used as photoanode material, as they are more stable under illumination [8]. On the other hand, in order to avoid possible photo-corrosion, narrow band gap materials are not used. Increase in the concentration of dye, enhancing the dye loading across the cross section and introduction of light scattering layers over the active layer for improved light harvesting are the different strategies available to enhance the energy conversion efficiency of the DSSCs [11,12]. However, the former is not preferred as thick dye layer attains insulating nature by mutual interaction among the excited molecules [13], and it gets de-activated. So, to attain high dye loading capacity without increasing the concentration, high surface area mesoporous wide bandgap semiconductor materials are preferred [9]. The widely known semiconductor materials which are active in visible region such as GaAs, CdS, Si and InP have been tried as photoanode, but due to the problem of photo corrosion with the above-mentioned materials the long-term stability of the solar cells could not be achieved. Some of the other commonly studied wide bandgap photoanode materials are ZnO, TiO_2, SnO_2, Nb_2O_5, Zn_2SnO_4. Though ZnO has higher electron mobility and has identical band position as TiO_2, due to its instability in acidic dye it is not the preferred choice for commercialisation. SnO_2 have also been used as photoanodes in DSSC, though it has higher mobility due to its rapid recombination and poor open circuit voltage, surface treatments were required for SnO_2 to be used as photoanode in DSSC. Other materials such as Nb_2O_5, Zn_2SnO_4, Fe_2O_3 have also been used as photoanodes in DSSC [14–18]. Among the different materials, TiO_2 is generally the material of choice due to its superior properties such as the position of the conduction band (as the TiO_2 conduction band lies lower to the LUMO (lowest unoccupied molecular orbital) level of the most of the commonly used organic dyes, providing feasibility for faster electron transfer), low toxicity, high chemical stability, high refractive index (which is essential for the light to diffuse into the whole mesoporous network) and high dielectric constant (which reduces the fast recombination of the electrons at the TiO_2/dye interface site through electrostatic shielding) [19–21].

Among the commonly studied phases of TiO_2 such as anatase, rutile and brookite, all of these have been used as photoanode in DSSC. As the anatase phase has the properties such as indirect bandgap, which does not favor direct transition of electrons from conduction to the valence band and this provides an order of magnitude higher lifetime for photogenerated electrons compared to rutile and brookite. Also, recombination of photogenerated carriers in anatase is slightly less as it is reported to have smaller photocarrier effective mass which could assist their fast migration [8,22,23].

Most commonly used methods for the synthesis of TiO_2 nanoparticles are sol-gel, Hydrothermal, Solvothermal, Microwave-assisted synthesis, green synthesis and template assisted methods [24–28]. Of the above-said techniques, hydrothermal/solvothermal technique is preferred by many of the researchers to prepare mesoporous metal oxides as it requires considerably lower reaction temperature as it can attain higher solubility and reactivity in the reaction medium at high pressures inside the autoclave. Additionally, it also has better control of morphology (narrow size distribution) of the prepared material [29–31]. On the other hand, microwave-assisted synthesis possesses advantages such as quick reaction time, efficient heating method, which uses the molecular vibrations of the dipole moment to produce rapid energy in the form of heat [32–34]. The choice of solvent is vital in microwave-assisted technique, and the polar solvents with loss tangent value ($\tan \delta$) > 1 have an excellent reactivity under microwave irradiation [35].

The objective of the present work is that though many works are available on the preparation of TiO_2 by solvothermal or microwave methods, the experiment conditions such as reaction time and temperature, choice of solvent and precursor are not virtually same. In this work, using the same initial precursors TiO_2 nanoparticles have been synthesized by solvothermal, and microwave methods and a direct comparison of the properties of synthesized TiO_2 and its performance as DSSC photoanode have been studied.

Experimental procedure

Preparation of precursor for the reaction

In this typical procedure, titanium tetraisopropoxide and anhydrous ethanol were used as the precursor and solvent, respectively. Initially, 0.1 M of TTIP was added to 30 mL of ethanol and was stirred for 1 h to obtain a clear solution. To the solution mentioned above 20 mL ethanol/deionized water mixture of 1:1 ratio was added, and instantaneously milky white solution was formed confirming the rapid hydrolysis of titanium precursors towards the formation of TiO_2. The obtained colloidal solution was further treated by solvothermal and microwave methods.

Solvothermal method growth of TiO_2 nanoparticles (NPs)

The solvothermal method was used to prepare TiO_2 nanoparticles (NPs). The white colored solution obtained was then transferred into a reagent bottle, and it was tightly sealed and subjected to solvothermal growth at 90 °C for 6 h. The final product was centrifuged, and it was further washed a few times with de-ionized water to remove the residual carbon from the solvent traces and was dried overnight at 120 °C. They were further annealed at 450 °C for 1 h.

Microwave-assisted preparation of TiO_2 nanoparticles

Milestone ETHOS1 Advanced Microwave Digestion System (Milestone, 2.5 GHz, sensor ATC-400) was used for the microwave assisted solvothermal synthesis of TiO_2 nanoparticles. The prepared precursor solution was transferred to a Teflon lined microwave digestion vessel which was sealed before the reaction. During the reaction, the microwave was ramped to obtain a temperature of 200 °C in first 15 min, and it was maintained at the same temperature for the next 30 min, before cooling to room temperature. The temperature was controlled using a temperature sensor in the first reaction vessel, and all the other reaction vessels had external temperature control using an IR sensor. Precipitates were collected by centrifugation after the reaction, and they were further dried overnight at 120 °C in a conventional oven, and it was used for further characterization and construction of DSSC.

Characterization techniques

The structural characteristics was analyzed using X-ray diffractometer (PANalytical XPERT-PRO) operating with Cu K$\propto$ radiation in a $\theta-2\theta$ geometry and the Raman spectra was recorded using a micro Raman spectrometer (EZRAMAN, Model: 5B1S-162) using 532 nm laser source. The optical absorption spectra were recorded using UV–Visible spectrophotometer (Jasco V-670). The photoluminescence (PL) and its lifetime measurements (TRPL) was carried out using Horiba, Fluorolog. The surface morphology was analyzed using field-emission scanning electron microscope (FE-SEM, ZEISS, SIGMA, UK). High resolution transmission electron microscope (HRTEM) images of the prepared samples have been recorded using a JEOL, JEM 2100 electron microscope. X-ray photoelectron Spectroscopy (XPS) studies were carried out using ESCA2000 (VG microtech: UK). Brunauer–Emmett–-Teller (BET) analysis was performed using ASAP 2020 micromeritics. The solar cell power conversion efficiency measurements for the fabricated cells was carried out using Keithley 2420 source meter under illumination of 1 Sun with an ORIEL Solar Simulator composed of 1000 W Xenon arc lamp with AM 1.5 and G filters. Active cell area was 0.25 cm^2. EIS measurements were carried out using CHI600 electrochemical analyzer under open circuit condition.

DSSC fabrication

As the first step, TiO_2 paste was prepared by the following method. Prepared nanoparticles were well ground, and it was mixed along with diluted acetic acid followed by addition of deionized water and was ground in a mortar until the paste attains homogeneity. Further 5% ethyl cellulose in ethanolic solution was added to the paste, and it was ground well. Finally, terpinol was added and it was further stirred until the paste attains homogeneity and in-order to remove ethanol from the mixture it was kept in a water bath at 90 °C for 10 min. The final prepared paste was coated over 40 mM $TiCl_4$ treated FTO (Fluorine doped Tin Oxide) by doctor blade method using the template spacers (an active surface area of 0.25 cm^2 and the total thickness of about 11 μm was optimized). The prepared photoanodes were further annealed at 450 °C for 30 min in a programmable muffle furnace at the rate of 10 °C/min. As the final step of photoanode preparation, when the prepared electrodes were around 80 °C (to avoid moisture at the surface), it was taken out of the furnace, and it is soaked in ethanolic 0.3 mM N719 dye (Solaronix) solution at room temperature for 12 h to remove the excess un-anchored dye molecules present on the surface, the sensitized electrodes were washed carefully with anhydrous ethanol and were dried. For the construction of DSSC, Pt sputtered FTO (Dyesol) was used as a counter electrode, Iodine redox (Iodolyte HI-30, Solaronix) was used as the electrolyte. The electrodes were sealed using a sealant, and the electrolyte was injected through the pre-drilled hole in the counter electrode, and the hole was then sealed using additional sealant.

Result and discussion

The XRD patterns of the TiO_2 samples synthesized by solvothermal synthesis (SS) and microwave assisted solvothermal synthesis (MWST) techniques are shown in Fig. 1. The diffraction patterns of TiO_2 nanoparticles prepared by both methods exhibit good crystalline peaks, and they correspond to the anatase phase of TiO_2. The diffraction peaks corresponding to the planes match well with the peaks corresponding to the anatase phase of TiO_2 (JCPDS Card No: 21-1272, shown as vertical lines in Fig. 1). From the graph, it could be inferred that with sharp peaks, the crystalline nature of the microwave prepared particles was found to be slightly more compared to that of TiO_2 nanoparticles prepared by solvothermal method. A small hump at 2θ, 30° (marked using '#' symbol in Fig. 1) corresponding to the brookite phase was

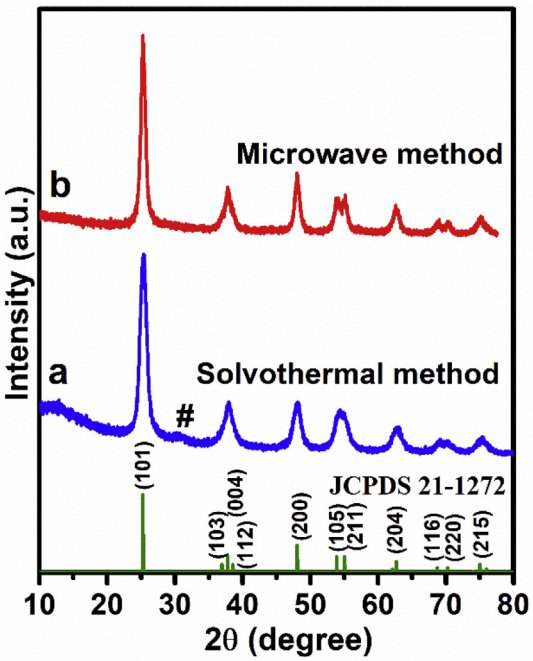

Fig. 1 – X-ray diffraction patterns of TiO_2 nanoparticles prepared by (a) solvothermal and (b) microwave assisted solvothermal techniques.

observed for the TiO_2 samples prepared by solvothermal method, and this small shoulder peak has been observed by other researchers as well [36]. It could be further noticed that TiO_2 nanoparticles prepared by both the methods have the tetragonal crystal structure with predominant broad diffraction peaks located at the Bragg diffraction angles (2θ) of 25.36, 37.79 48.14, 53.89, 55.12, 62.63, 68.84, 70.51 and 75.11 which are indexed to (101), (004), (200), (105), (211), (204), (116), (220) and (215) lattice planes respectively [37].

TiO_2 has a tetragonal structure, and it belongs to the space group D_{4h}^{19} (I4/amd). According to the factor group analysis, the 15 optical modes have the irreducible representation $1A_{1g} + 1A_{2u} + 2B_{1g} + 1\ B_{2u} + 3\ E_g + 2\ E_u$. Among which, A_{1g}, B_{1g}, E_g are Raman active modes, A_{2u} and E_u are infrared active modes, B_{2u} is inactive in both [38]. Nanocrystalline anatase TiO_2 material consists of six active vibrational Raman modes, expressed as $[A_{1g} + 2B_{1g} + 3E_g]$, where A_{1g}, B_{1g} are nondegenerate modes and Eg is a doubly degenerate mode [39,40]. The Raman spectra of the prepared TiO_2 is shown in Fig. 2. The first high intensity peak observed at 144 and 147 cm^{-1} for ST and MWST samples, correspond to the E_{1g} mode, which is attributed to the stretching modes of Ti–O bond. B_{1g} mode at 398 and 397 cm^{-1} accordingly for the TiO_2 prepared by ST and MWST methods represents bending modes of O–Ti–O bond, the peaks at 520 and 516 cm^{-1} for ST and MWST samples represents the overlapping of A_{1g} and B_{1g} modes and these modes are generally assigned to symmetric and antisymmetric bending modes of O–Ti–O bond. Peaks at 642 and 640 cm^{-1} for ST and MWST samples correspond to the E_g mode [41]. Here the corresponding peaks of MWST samples were slightly blue shifted and the broadening of peaks were observed when compared to that of ST method prepared sample. By the law of conservation, with the reduction in the

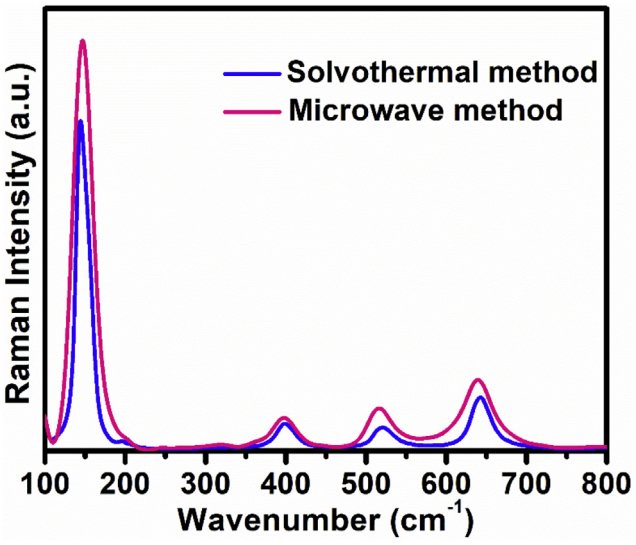

Fig. 2 – Raman spectra of TiO_2 nanoparticles prepared by solvothermal and microwave assisted solvothermal techniques.

grain size, the phonon momentum distribution increases and this leads to the asymmetric broadening, which is expected to be the cause behind the shift in Raman lines [38]. Further, it is observed from the spectrum that the prepared material is free from any secondary peaks corresponding to the other polymorphs of the TiO_2.

UV–Vis absorption spectra are shown in Fig. 3. UV–Vis absorption range of the TiO_2 nanoparticles prepared by both the methods is found to be in shorter wavelength region, and this kind of behavior is associated with wide bandgap semiconductors [42]. Fig. 3 Shows the UV–Vis absorption spectra of the TiO_2 synthesized by ST and MWST methods. The absorption edge was evident from Fig. 3, and the value was found to be 399 nm and 391 nm for the TiO_2 nanoparticles

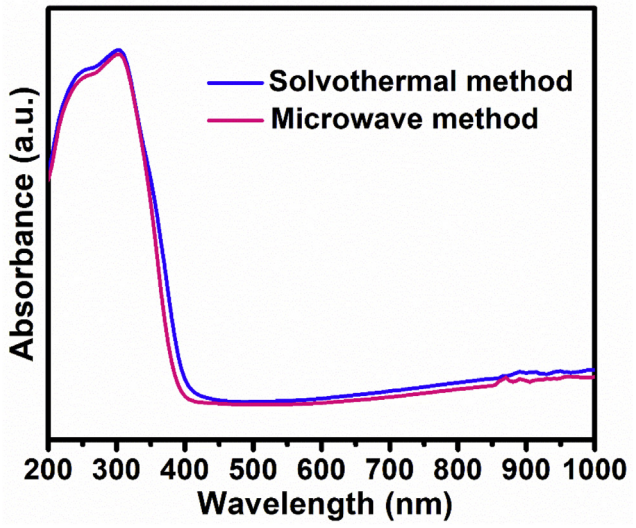

Fig. 3 – UV–Vis absorption spectra of TiO_2 nanoparticles prepared by solvothermal and microwave assisted solvothermal techniques.

prepared by ST and MWST methods, respectively. From the absorbance band edge, the band gap of TiO_2 nanoparticles prepared by ST and MWST methods were calculated using the formula $E_g = 1239.8/\lambda$. Here E_g represents the band gap (eV) and λ (nm) represents absorption edge wavelength [43]. The band gap values are calculated and found to be 3.11 and 3.17 eV for the samples prepared by ST and MWST methods respectively. The bandgap was found to be slightly lower for the TiO_2 prepared by solvothermal method, which could be due to the presence of oxygen vacancies [44].

Photoluminescence emission spectra of the TiO_2 nanoparticles prepared by ST and MWST methods (Fig. 4a) was recorded using the excitation wavelength of 280 nm. From the spectra, strong UV emission which is characteristic of wide bandgap semiconducting oxide materials was observed for both the samples. Another emission was observed at 460 nm, which corresponds to the oxygen vacancies [45]. The time spent by the excited atom or molecule in the excited state before emitting a photon and returning to the ground state is generally known as Fluorescence lifetime (FLT), and this can vary from picoseconds to microseconds depending on the material. To study the carrier transfer in the TiO_2 prepared by ST and MWST methods, time-resolved photoluminescence studies (TRPL) were carried out under the excitation and emission values of 280 and 380 nm, respectively. Fig. 4b shows the TRPL decay curves of the TiO_2 prepared by ST and MWST methods. From the graph, it can be inferred that both curves are slightly different, and they do not follow the same pattern. This decay is a multiexponential process with different short and long components. The decay curves follow tri-exponential decay function and are best fitted with the following expression [46].

$$R(t) = A_1 e^{-t/\tau_1} + A_2 e^{-t/\tau_2} + A_3 e^{-t/\tau_3} \quad (1)$$

Here, $\tau_1$and τ_2 represents the fast decay components, and $A_1$and A_2 are their relative amplitudes of fast decay. τ_3 represents slow decay component of the lifetime and A_3 is the relative amplitude of slow decay [47]. Free exciton states contribute to the fast decay, and the bound ones contribute to the slow decay components, respectively. The derived relative components contribution from the fast and slow decay components are given in Table 1.

The distinct emission decay components provide a hint about various exciton recombination paths. From the calculated values tabulated in Table 1, we could infer that the fast decay component relative intensity of the TiO_2 prepared by microwave is less compared to solvothermal prepared one, and this could be related to lower recombination. The average PL lifetime (τ) of the TiO_2 prepared by different methods were calculated by the formula [47,48].

$$\tau = \frac{A_1\tau_1^2}{A_1\tau_1} + \frac{A_2\tau_2^2}{A_2\tau_2} + \frac{A_3\tau_3^2}{A_3\tau_3} \quad (2)$$

The symbols here represent the same as discussed in the above equation. The average PL lifetime was calculated to be 11.34 and 13.56 ns respectively for solvothermal, and microwave (ST and MWST) synthesized TiO_2 respectively.

FE-SEM and HRTEM images of the TiO_2 samples prepared by two different methods are shown in Fig. 5. FE-SEM images of the TiO_2 prepared by solvothermal method (ST) (Fig. 5 (a)) shows the presence of near-spherical shape particles, and the samples prepared by microwave-assisted method (MWST) (Fig. 5 (b)) exhibits aggregates like structure, which on further examination by TEM analysis, showed that it might be the result of agglomerated nanoparticles. The lower magnification TEM micrographs of TiO_2 prepared by solvothermal method (ST) (Fig. 5 (c, e)) shows near uniform spherical shaped particles, and from the higher magnification image lattice fringes were observed. In the case of microwave method (MWST), it was found to show agglomerated nanoparticles (Fig. 5 (d, f)) which may be due to the rapid reaction which occurs in the microwave method. The distance of separation (d) between two successive lattice fringes is obtained from the high magnification TEM images and the value was calculated to be 0.352 (Fig. 5 (g)) and 0.354 nm (Fig. 5 (i)) respectively for the samples synthesized by solvothermal and microwave methods. The obtained d-spacing value corresponds to the (101) plane of TiO_2 anatase phase [42]. The polycrystalline nature of the prepared samples was inferred from the selected area electron diffraction (SAED) pattern, which shows distinct ring patterns (Fig. 5 (h) and 5 (j)).Using the SAED pattern, the d-spacing values are calculated and the calculated d-spacing values corresponding to the (h k l) planes of (101), (004), (200), (211) and (204), which agrees with the XRD results [49]. The

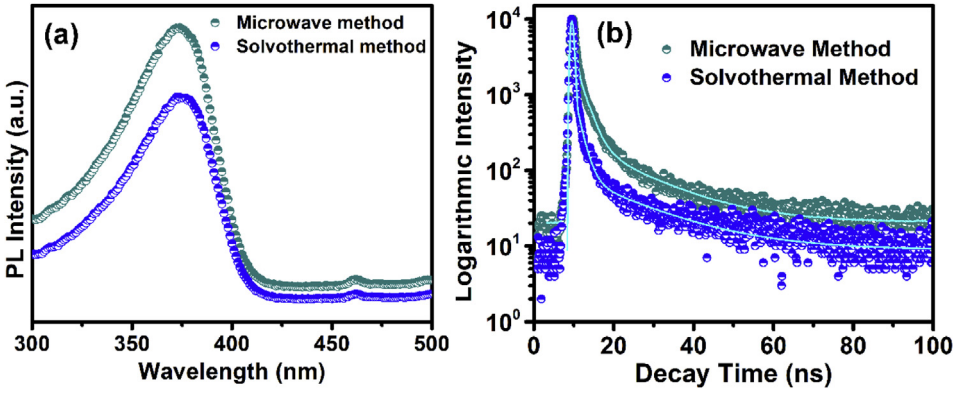

Fig. 4 – (a) Photoluminescence spectra and (b) transient decay curves of TiO_2 nanoparticles prepared by solvothermal and microwave assisted solvothermal methods.

Table 1 – The best-fit parameters of PL decay curves of TiO_2 nanoparticles prepared by solvothermal and microwave assisted solvothermal techniques.

Sample	τ_1 (ns)	τ_2 (ns)	τ_3 (ns)	A_1 (%)	A_2 (%)	A_3 (%)	Average lifetime τ_{av} (ns)
Solvothermal	0.1270	1.5931	16.8415	81.43	11.92	6.65	11.34
Microwave	0.1439	2.1232	14.5994	60.93	26.22	12.85	13.56

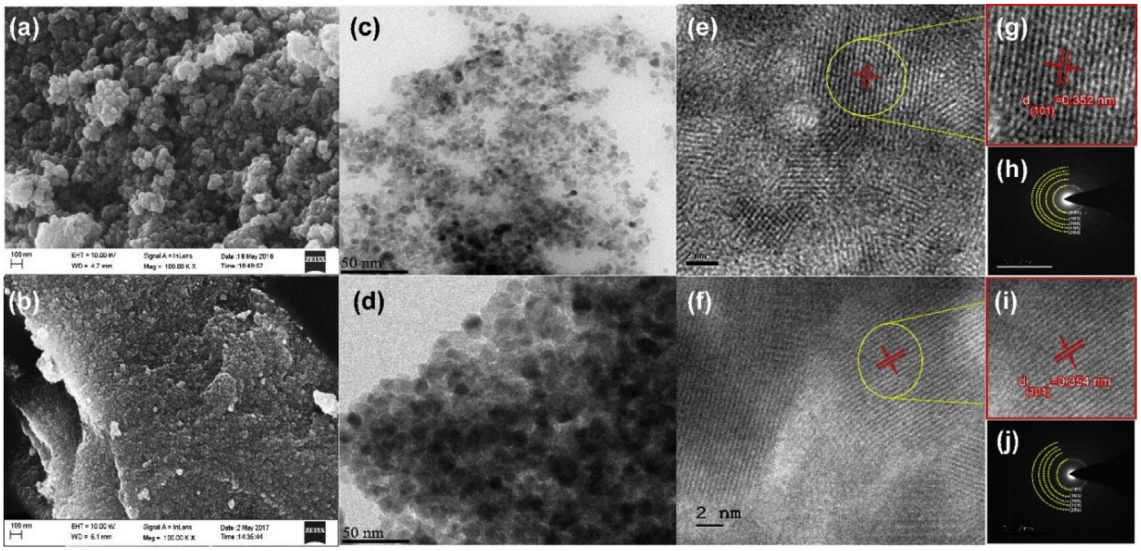

Fig. 5 – FESEM images of TiO_2 nanoparticles prepared by (a) solvothermal and (b) Microwave method. HRTEM micrographs of TiO_2 nanoparticles prepared by (c, e) solvothermal and (d, f) Microwave method.

corresponding particles size distribution histogram fitted to the Gaussian distribution function of TiO_2 synthesized by solvothermal and microwave methods is given in Fig. 6. From the histogram the average particle size was found to be in the range of 6.1 to 8.9 nm for the TiO_2 synthesized by ST and MWST methods respectively.

In dye-sensitized solar cells the amount of dye adsorbed over the surface of the semiconductor is important, the surface is one of the essential part, as this plays an essential role in determining the efficiency of the solar cells. In Brunauer–Emmett–Teller (BET) analysis, N_2 adsorption and desorption isotherm gives information about the surface area of the material and Barrett–Joyner–Halenda (BJH) analysis gives information about the pore size distribution. From Fig. 7a it can be observed that in the case of both solvothermal (ST) and microwave (MWST) methods the BET loop exhibits type IV according to IUPAC classification and it falls under H_2 type hysteresis loop indicating the existence of cylindrical shaped mesopores [50,51] and further the mesoporous characteristics of the prepared TiO_2 nanomaterials can be confirmed from the presence of relatively higher-pressure range hysteresis loop ($P/P_0 > 0.5$) [52]. The specific surface

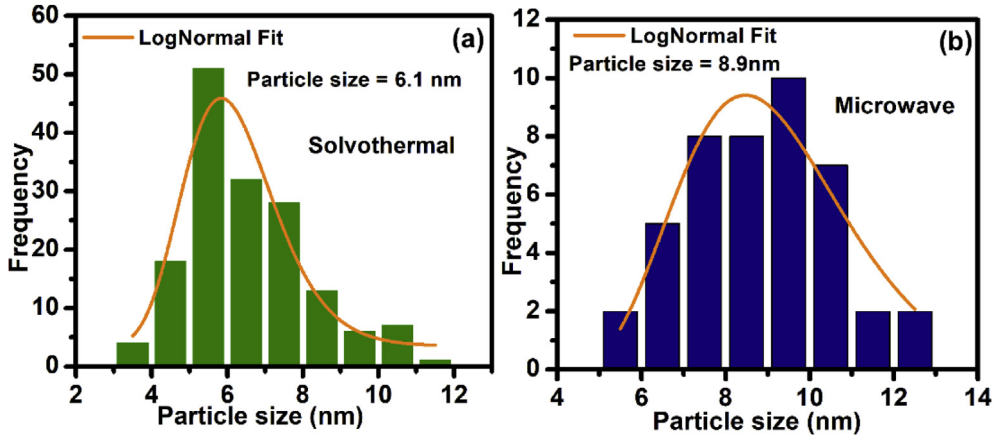

Fig. 6 – Particle size histogram of the TiO_2 nanoparticles synthesized by solvothermal and microwave methods.

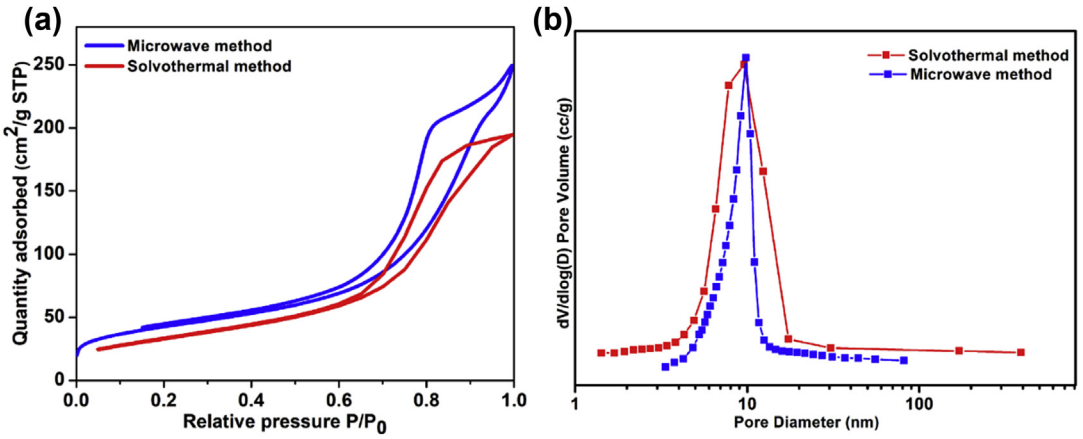

Fig. 7 – (a) N_2 adsorption-desorption isotherms, and (b) corresponding pore diameter distribution curves of TiO_2 nanoparticles prepared by solvothermal and microwave assisted solvothermal techniques.

area of TiO_2 prepared by solvothermal and microwave methods was found to be 113.9 m^2/g and 116.1 m^2/g. From the Barrett–Joyner–Halenda (BJH) analysis, pore size distribution (Fig. 7b) exhibits a sharp peak, signifying the presence of comparatively uniform pore size. The average pore diameter and pore volume was found to be 7.8 nm and 0.296 cc/g for the TiO_2 prepared by solvothermal (ST) method and 9.3 nm and 0.373 cc/g for the microwave (MWST) prepared TiO_2 respectively.

X-ray photoelectron spectroscopy (XPS) analysis was carried out to further examine the chemical states of the prepared material at the surface and sub-surface level (up to 3 nm). In the survey spectra shown in Fig. 8a, the photoelectron signals corresponding to Ti, O and C elements were observed. The occurrence of C1s peak in the samples prepared by both methods (ST and MWST) is owed to the exposure of the samples to the atmosphere and could also be due to the traces of the solvent present [53]. From the core-level spectrum of Ti 2p (Fig. 8b), the binding energy values (BE) for the Ti $2p_{1/2}$ and Ti $2p_{3/2}$ were observed at 464.3 and 458.6 eV for the ST sample, and it was observed for the MWST sample at 464.4 and 458.6 eV and these two peaks in both the samples correspond to the Ti^{4+} of TiO_2 [54]. The peaks for T^{3+} were not observed. The O1s spectra of the ST and MWST samples are shown in Fig. 8c and d respectively. It is deconvoluted using a Gaussian fit. Two peaks at 529.82 and 531.15 eV corresponding to Ti–O surface species and adsorbed hydroxyl groups were observed for the ST samples (Fig. 8c). For the sample prepared by microwave method (Fig. 8d), the three peaks present at 529.1, 530.67 and 531.33 eV correspond to that of lattice oxygen, Ti–O–Ti surface species and surface hydroxyl groups respectively [53].

The fabricated solar cells charge transport properties were analyzed by Impedance spectroscopy; the measurements were recorded under dark with 0.6 V as applied bias. From the Nyquist plot (Fig. 9a), the semicircle observed in the mid-frequency region could be ascribed to the charge transfer resistance of the TiO_2/dye/electrolyte interface [55]. They were further fitted using the equivalent circuit and the model circuit is presented as inset, its series resistance (R_s) and charge transfer resistance (R_{ct}) and a CPE element (used instead capacitor to compensate for non-homogeneity in the system) connected in parallel are given in Table 2. From Table 2 it can be inferred that under the dark condition no electrons can be injected from the sensitizer into TiO_2 site, electrons here have to move through the interconnected TiO_2 network before their reaction with the electrolyte and the charge-transfer resistance (Rct) here at the TiO_2/sensitizer/electrolyte interface infers the recombination resistance. The values were found to be 190.4, 224.4, 299.2 Ω for P25, ST and MWST samples respectively. The higher value for the MWST sample infers that it is better in retarding the recombination.

Further, from the Bode plots (Fig. 9b) the peak in the high-frequency region is connected to the R_{ct} of the fabricated solar cells, where higher frequency and smaller phase value peaks often indicate lower R_{ct}. The MWST sample showed less phase value compared to ST sample. The electron lifetimes (τ_e) are determined from the Bode phase plots using the following equation [52];

$$\tau_e = 1/2\pi f_{max} \quad (3)$$

where f_{max} is the maximum peak frequency in the middle frequency range. The electron lifetime was calculated to be 1.2 ms (ms) and 0.98 ms (ms) for the MWST and ST samples respectively. The amount of dye adsorbed by the TiO_2 anodes was calculated by dye desorption measurements. It was carried out by immersing the dye adsorbed photoanode into a fixed volume of 0.1 M NaOH, during this process the dye gets desorbed. UV–VIS absorption measurements were carried out for the desorbed dye and by using the Beer Lambert's law the concentration of dye adsorbed were calculated. And the calculated values were tabulated in Table 2. Fig. 10 shows the current density-voltage (J-V) curves of the device fabricated using TiO_2 prepared using the two methods described above and for comparison, solar cells were also fabricated using the commercial TiO_2 (P25) and their performances were compared. The TiO_2 device prepared by solvothermal (ST) method exhibited power conversion efficiency (η) of 5.98%, (open-circuit voltage (V_{oc}) = 0.713 V, short-circuit current density (J_{SC}) = 12.72 mA, fill factor (FF) = 66%), the device constructed using TiO_2 prepared by microwave (MWST) method exhibited power conversion efficiency (η) of

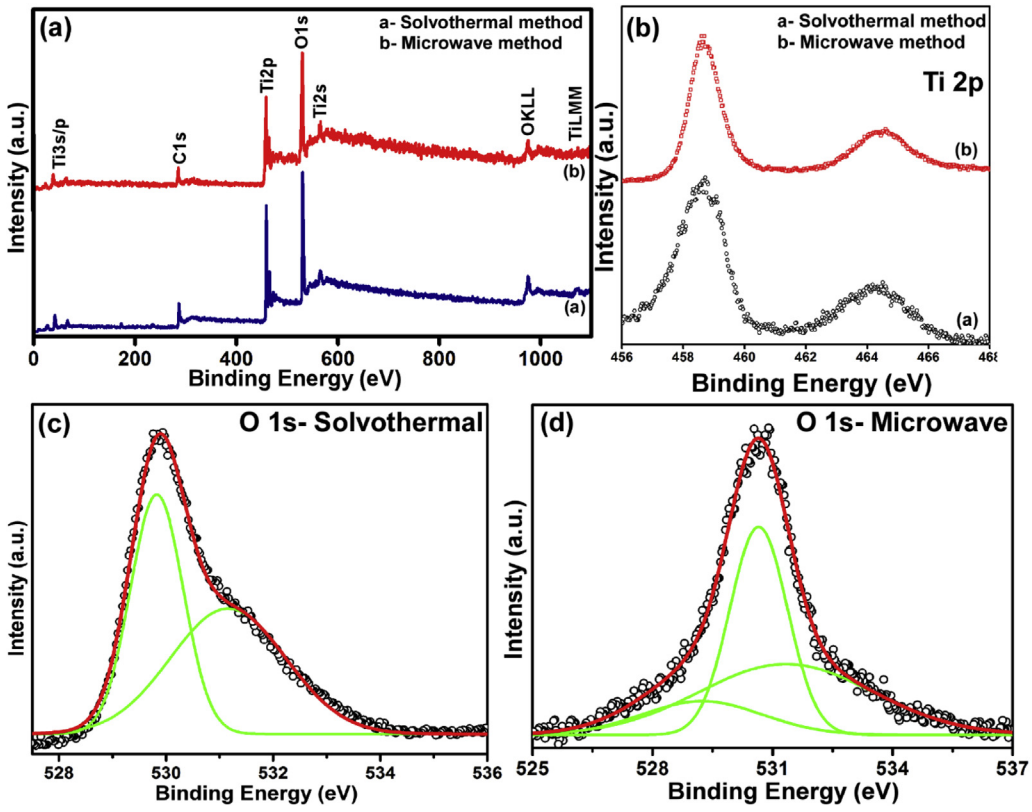

Fig. 8 – (a) XPS survey spectra, (b) core level XPS spectra of Ti 2p, (c) core level XPS spectra of O 1s and (d) core level XPS spectra of O 1s of TiO_2 nanoparticles prepared by solvothermal and microwave methods respectively.

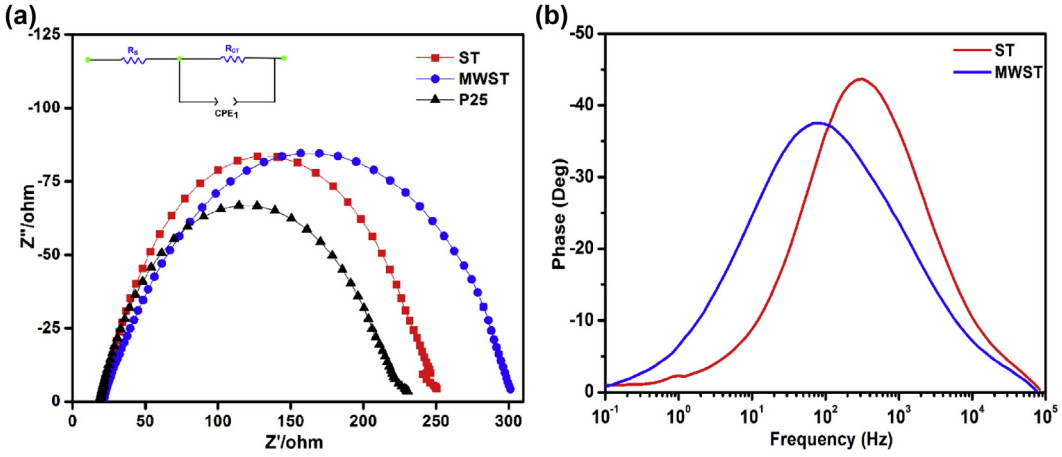

Fig. 9 – (a) Nyquist plots and (b) Bode-phase plots of TiO_2 nanoparticles prepared by solvothermal and microwave assisted solvothermal techniques.

7.44% (open-circuit voltage (V_{oc}) = 0.732 V, short-circuit current density (J_{SC}) = 14.52 mA, fill factor (FF) = 70%) and the device fabricated using the commercial TiO_2 (P25) exhibited power conversion efficiency (η) of 4.12%, (open-circuit voltage (V_{oc}) = 0.698 V, short-circuit current density (J_{SC}) = 9.68 mA, fill factor (FF) = 61%) respectively. The improvement in the power conversion efficiency of the microwave prepared samples (MWST) could be ascribed to the parameters such as enhanced surface area for the MWST samples compared to the TiO_2 prepared by solvothermal method (ST). Further, its uniform pore distribution could pave the way for better electrolyte diffusion into the TiO_2 network. Interconnected particles and porous nature were observed from the TEM image of the MWST sample, this interconnectivity between the particles reduces the grain boundaries which are essential for a faster electron transport and to decrease recombination losses [56]. From the impedance analysis results it could further be inferred that the recombination resistance was found to be higher for the MWST sample compared to ST and P25 samples [57]. The slight decrease in V_{OC} for the P25 samples could be

Table 2 – Parameters calculated from IV measurement and EIS spectra of the constructed DSSC with three different TiO_2 photoanodes.

Sample	V_{OC} (mV)	J_{SC} (mA)	FF (%)	η (%)	R_S (Ω)	R_{CT} (Ω)	CPE-P	Dye loading (× 10^{-6}) mol cm^{-2}
P25	0.698	9.68	61	4.12	19.12	190.4	0.8087	6.44
Solvothermal	0.713	12.72	66	5.98	21.14	224.4	0.8086	8.43
Microwave	0.732	14.52	70	7.44	20.96	299.2	0.6607	9.34

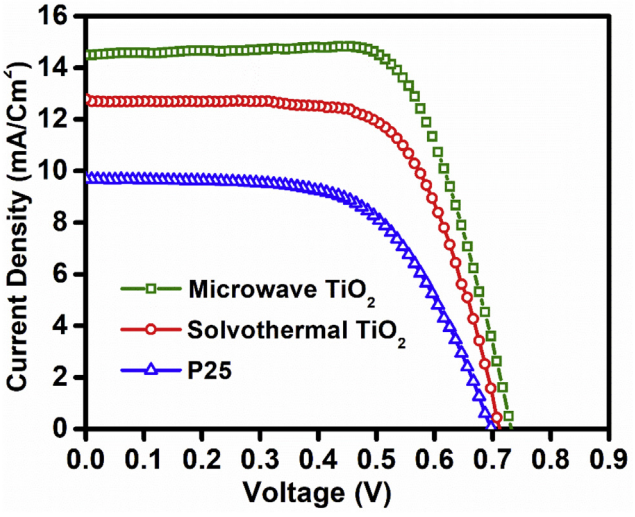

Fig. 10 – J-V curves of the solar devices fabricated using TiO_2 nanoparticles prepared by solvothermal and microwave assisted solvothermal techniques.

due to the presence of rutile phase in the P25 (TiO_2) powder, which causes the shift in the band and the decrease in short-circuit current may be due to its lower dye adsorption owing to its lower surface area [58]. The efficiency of the TiO_2 prepared by solvothermal method was found to be slightly less compared to microwave assisted technique, which could also be due to the presence of excessive oxygen vacancies.

Conclusions

Here in this work, TiO_2 nanoparticles were prepared by microwave and solvothermal methods and its comparative study have been carried out. From the X-ray diffraction pattern and Raman spectra it is observed that the prepared TiO_2 is of anatase phase. The optical properties of the prepared materials were analyzed by using UV absorption and photoluminescence spectra and the results show strong absorption in shorter wavelength region in the UV spectra and a strong UV emission is observed from the PL spectra respectively. The TEM images of the TiO_2 nanoparticles prepared by solvothermal method shows the presence of near spherical shape particles and aggregate type morphology was observed for the TiO_2 nanoparticles prepared by microwave method. The Brunauer–Emmett–Teller (BET) analysis of the TiO_2 prepared by both the methods reveal that the materials are of mesoporous nature and from the Barrett–Joyner–Halenda (BJH) pore size distribution curve it is observed to be unimodal type of distribution. The chemical states of the prepared materials were studied using XPS analysis. Dye-sensitized solar cells were constructed with the structure FTO/TiO_2-Dye/redox electrolyte/Pt-FTO and their electrochemical performance were studied by EIS in the dark, its efficiency was analyzed under standard one sun intensity using a solar simulator. The DSSCs constructed using microwave prepared nanoparticles as active layer exhibited a maximum power conversion efficiency of 7.44%.

Declaration of competing interest

The authors declare that they have no known competing financial interests or personal relationships that could have appeared to influence the work reported in this paper.

Acknowledgement

Author VMR would like to thank Prof. P. Ravirajan, University of Jaffna, Sri Lanka for his insightful suggestions to the manuscript. Authors gratefully acknowledge the financial support provided by the Indo-Norwegian Collaborative Project INCP and UTFORSK Program.

REFERENCES

[1] Fan K, Yu J, Ho W. Improving photoanodes to obtain highly efficient dye-sensitized solar cells: a brief review. Mater Horiz 2017;4:319–44.
[2] Mohamed IMA, Dao V-D, Yasin AS, Choi H-S, Barakat NAM. Synthesis of novel SnO_2@TiO_2 nanofibers as an efficient photoanode of dye-sensitized solar cells. Int J Hydrogen Energy 2016;41:10578–89.
[3] Pitchaiya S, Natarajan M, Santhanam A, Asokan V, Yuvapragasam A, Madurai Ramakrishnan V, et al. A review on the classification of organic/inorganic/carbonaceous hole transporting materials for perovskite solar cell application. Arabian J Chem 2020;13:2526–57.
[4] Zheng H, Li C, Wei A, Liu J, Zhao Y, Xiao Z. Study of carbon-based hole-conductor-free perovskite solar cells. Int J Hydrogen Energy 2018;43:11403–10.
[5] Pitchaiya S, Eswaramoorthy N, Natarajan M, Santhanam A, Ramakrishnan VM, Asokan V, et al. Interfacing green synthesized flake like-ZnO with TiO2 for bilayer electron extraction in perovskite solar cells. New J Chem 2020;44:8422–33.
[6] Ghann W, Sharma V, Kang H, Karim F, Richards B, Mobin SM, et al. The synthesis and characterization of carbon dots and their application in dye sensitized solar cell. Int J Hydrogen Energy 2019;44:14580–7.

[7] Jiang Q-S, Cheng W, Wu J, Li W, Zhu J, Zhu Y, et al. In situ electrodeposition of nickel cobalt selenides on FTO as an efficient counter electrode for dye-sensitized solar cells. Int J Hydrogen Energy 2019;44:23936–46.
[8] Kay A, Grätzel M. Low cost photovoltaic modules based on dye sensitized nanocrystalline titanium dioxide and carbon powder. Sol Energy Mater Sol Cell 1996;44:99–117.
[9] Barbé CJ, Arendse F, Comte P, Jirousek M, Lenzmann F, Shklover V, et al. Nanocrystalline titanium oxide electrodes for photovoltaic applications. J Am Ceram Soc 1997;80:3157–71.
[10] Riaz R, Ali M, Maiyalagan T, Arbab AA, Anjum AS, Lee S, et al. Activated charcoal and reduced graphene sheets composite structure for highly electro-catalytically active counter electrode material and water treatment. Int J Hydrogen Energy 2020;45:7751–63.
[11] Madurai Ramakrishnan V, Sandberg S, Muthukumarasamy N, Kvamme K, Balraju P, Agilan S, et al. Microwave-assisted solvothermal synthesis of worms-like TiO_2 nanostructures in submicron regime as light scattering layers for dye-sensitized solar cells. Mater Lett 2019;236:747–51.
[12] Chava RK, Lee W-M, Oh S-Y, Jeong K-U, Yu Y-T. Improvement in light harvesting and device performance of dye sensitized solar cells using electrophoretic deposited hollow TiO_2 NPs scattering layer. Sol Energy Mater Sol Cell 2017;161:255–62.
[13] Tennakone K, Kumara GRRA, Kumarasinghe AR, Wijayantha KGU, Sirimanne PM. A dye-sensitized nano-porous solid-state photovoltaic cell. Semicond Sci Technol 1995;10:1689–93.
[14] Chava RK, Raj S, Yu Y-T. Synthesis and electrophoretic deposition of hollow-TiO_2 nanoparticles for dye sensitized solar cell applications. J Alloys Compd 2016;672:212–22.
[15] Ramakrishnan VM, Muthukumarasamy N, Palraju B, Pitchaiya S, Velauthapillai D, Pugazhendhi A. Transformation of TiO_2 nanoparticles to nanotubes by simple solvothermal route and its performance as dye-sensitized solar cell (DSSC) photoanode. Int J Hydrogen Energy 2020;45(31):15441–52.
[16] Masjedi-Arani M, Salavati-Niasari M. Simple size-controlled fabrication of Zn_2SnO_4 nanostructures and study of their behavior in dye sensitized solar cells. Int J Hydrogen Energy 2017;42:858–66.
[17] Raj CC, Prasanth R. A critical review of recent developments in nanomaterials for photoelectrodes in dye sensitized solar cells. J Power Sources 2016;317:120–32.
[18] Yeoh M-E, Chan K-Y. Recent advances in photo-anode for dye-sensitized solar cells: a review. Int J Energy Res 2017;41:2446–67.
[19] Grätzel M. Perspectives for dye-sensitized nanocrystalline solar cells. Prog Photovoltaics Res Appl 2000;8:171–85.
[20] Cahen D, Hodes G, Grätzel M, Guillemoles JF, Riess I. Nature of photovoltaic action in dye-sensitized solar cells. J Phys Chem B 2000;104:2053–9.
[21] Luttrell T, Halpegamage S, Tao J, Kramer A, Sutter E, Batzill M. Why is anatase a better photocatalyst than rutile? - model studies on epitaxial TiO_2 films. Sci Rep 2014;4:4043.
[22] Park NG, van de Lagemaat J, Frank AJ. Comparison of dye-sensitized rutile- and anatase-based TiO_2 solar cells. J Phys Chem B 2000;104:8989–94.
[23] Magne C, Cassaignon S, Lancel G, Pauporté T. Brookite TiO_2 nanoparticle films for dye-sensitized solar cells. ChemPhysChem 2011;12:2461–7.
[24] Mamaghani AH, Haghighat F, Lee C-S. Hydrothermal/solvothermal synthesis and treatment of TiO_2 for photocatalytic degradation of air pollutants: preparation, characterization, properties, and performance. Chemosphere 2019;219:804–25.
[25] Wang Y, He Y, Lai Q, Fan M. Review of the progress in preparing nano TiO_2: an important environmental engineering material. J Environ Sci 2014;26:2139–77.
[26] Dufour F, Cassaignon S, Durupthy O, Colbeau-Justin C, Chanéac C. Do TiO_2 nanoparticles really taste better when cooked in a microwave oven? Eur J Inorg Chem 2012;2012:2707–15.
[27] Hariharan D, Jegatha Christy A, Pitchaiya S, Sagadevan S, Thangamuniyandi P, Devan U, et al. Green hydrothermal synthesis of gold and palladium doped titanium dioxide nanoparticles for multifunctional performance. J Mater Sci Mater Electron 2019;30:12812–9.
[28] Lee Y, Chae J, Kang M. Comparison of the photovoltaic efficiency on DSSC for nanometer sized TiO_2 using a conventional sol–gel and solvothermal methods. J Ind Eng Chem 2010;16:609–14.
[29] Darr JA, Zhang J, Makwana NM, Weng X. Continuous hydrothermal synthesis of inorganic nanoparticles: applications and future directions. Chem Rev 2017;117:11125–238.
[30] Archana J, Navaneethan M, Hayakawa Y. Solvothermal growth of high surface area mesoporous anatase TiO_2 nanospheres and investigation of dye-sensitized solar cell properties. J Power Sources 2013;242:803–10.
[31] Negi SS. Integrated electronic, optical, and structural features in pseudo-3D mesoporous TiO_2–X delivering enhanced dye-sensitized solar cell performance. ACS Omega 2018;3:1645–52.
[32] Rao KJ, Vaidhyanathan B, Ganguli M, Ramakrishnan PA. Synthesis of inorganic solids using microwaves. Chem Mater 1999;11:882–95.
[33] Umale SV, Tambat SN, Sudhakar V, Sontakke SM, Krishnamoorthy K. Fabrication, characterization and comparison of DSSC using anatase TiO_2 synthesized by various methods. Adv Powder Technol 2017;28:2859–64.
[34] Santhosh N, Govindaraj R, Pandian MS, Ramasamy P. Facile synthesis of mesoporous TiO_2 nanospheres by microwave-assisted hydrothermal method and its applications in dye sensitized solar cells. AIP Conference Proceedings 2017;1832:050003.
[35] Bilecka I, Niederberger M. Microwave chemistry for inorganic nanomaterials synthesis. Nanoscale 2010;2:1358–74.
[36] Kaur H, Kumar S, Verma NK, Singh P. Role of pH on the photocatalytic activity of TiO_2 tailored by W/T mole ratio. J Mater Sci Mater Electron 2018;29:16120–35.
[37] Shen P-S, Tai Y-C, Chen P, Wu Y-C. Clean and time-effective synthesis of anatase TiO_2 nanocrystalline by microwave-assisted solvothermal method for dye-sensitized solar cells. J Power Sources 2014;247:444–51.
[38] Ohsaka T, Izumi F, Fujiki Y. Raman spectrum of anatase, TiO_2. J Raman Spectrosc 1978;7:321–4.
[39] Ohsaka T, Yamaoka S, Shimomura O. Effect of hydrostatic pressure on the Raman spectrum of anatase (TiO_2). Solid State Commun 1979;30:345–7.
[40] Beattie IR, Gilson TR, Anderson John S. Single crystal laser Raman spectroscopy. Proc Royal Soc London Series A Math Phy Sci 1968;307:407–29.
[41] Xu CY, Zhang PX, Yan L. Blue shift of Raman peak from coated TiO_2 nanoparticles. J Raman Spectrosc 2001;32:862–5.
[42] Bakre PV, Tilve SG. Dicarboxylic acids as soft templates for the sol-gel synthesis of mesoporous nano TiO_2 with enhanced photocatalytic activity. Chemistry 2017;2:7063–72.
[43] Zhang H, Wu R, Xu H, Li F, Wang S, Wang J, et al. A simple spray reaction synthesis and characterization of hierarchically porous SnO_2 microspheres for an enhanced dye sensitized solar cell. RSC Adv 2017;7:12446–54.

[44] Wang X, Hu H, Yang Z, Kong Y, Fei B, Xin JH. Visible light-active sub-5nm anatase TiO_2 for photocatalytic organic pollutant degradation in water and air, and for bacterial disinfection. Catal Commun 2015;72:81–5.
[45] Liqiang J, Yichun Q, Baiqi W, Shudan L, Baojiang J, Libin Y, et al. Review of photoluminescence performance of nano-sized semiconductor materials and its relationships with photocatalytic activity. Sol Energy Mater Sol Cell 2006;90:1773–87.
[46] Selvaraj J, Mahesh A, Asokan V, Baskaralingam V, Dhayalan A, Paramasivam T. Phosphine-free, highly emissive, water-soluble Mn:ZnSe/ZnS core–shell nanorods: synthesis, characterization, and in vitro bioimaging of HEK293 and HeLa cells. ACS Applied Nano Materials 2018;1:371–83.
[47] Beura R, Pachaiappan R, Thangadurai P. A detailed study on Sn^{4+} doped ZnO for enhanced photocatalytic degradation. Appl Surf Sci 2018;433:887–98.
[48] Jayaraj SK, Sadishkumar V, Arun T, Thangadurai P. Enhanced photocatalytic activity of V_2O_5 nanorods for the photodegradation of organic dyes: a detailed understanding of the mechanism and their antibacterial activity. Mater Sci Semicond Process 2018;85:122–33.
[49] Venkatraman MR, Muthukumarasamy N, Balasundaraprabhu R, Agilan S, Velauthapillai D. Solvothermal synthesis of TiO_2/CNT composites and its physical and chemical properties. AIP Conference Proceedings 2015;1665:050166.
[50] Huang C-H, Yang Y-T, Doong R-A. Microwave-assisted hydrothermal synthesis of mesoporous anatase TiO_2 via sol–gel process for dye-sensitized solar cells. Microporous Mesoporous Mater 2011;142:473–80.
[51] Alwin S, Shajan XS, Karuppasamy K, Warrier KGK. Microwave assisted synthesis of high surface area TiO_2 aerogels: a competent photoanode material for quasi-solid dye-sensitized solar cells. Mater Chem Phys 2017;196:37–44.
[52] Wang X, Tian J, Fei C, Lv L, Wang Y, Cao G. Rapid construction of TiO_2 aggregates using microwave assisted synthesis and its application for dye-sensitized solar cells. RSC Adv 2015;5:8622–9.
[53] Bharti B, Kumar S, Lee H-N, Kumar R. Formation of oxygen vacancies and Ti^{3+} state in TiO_2 thin film and enhanced optical properties by air plasma treatment. Sci Rep 2016;6:32355.
[54] Tian Z, Cui H, Xu J, Zhu G, Shao F, He J, et al. Efficient charge separation of in-situ Nb-doped TiO_2 nanowires for photoelectrochemical water–splitting. Chemistry 2017;2:2822–7.
[55] Subalakshmi K, Senthilselvan J. Effect of fluorine-doped TiO_2 photoanode on electron transport, recombination dynamics and improved DSSC efficiency. Sol Energy 2018;171:914–28.
[56] Kondalkar VV, Mali SS, Pawar NB, Mane RM, Choudhury S, Hong CK, et al. Microwave-assisted rapid synthesis of highly porous TiO_2 thin films with nanocrystalline framework for efficient photoelectrochemical conversion. Electrochim Acta 2014;143:89–97.
[57] Song J, Yang HB, Wang X, Khoo SY, Wong CC, Liu X-W, et al. Improved utilization of photogenerated charge using fluorine-doped TiO_2 hollow spheres scattering layer in dye-sensitized solar cells. ACS Appl Mater Interfaces 2012;4:3712–7.
[58] Amoli V, Bhat S, Maurya A, Banerjee B, Bhaumik A, Sinha AK. Tailored synthesis of porous TiO_2 nanocubes and nanoparallelepipeds with exposed {111} facets and mesoscopic void space: a superior candidate for efficient dye-sensitized solar cells. ACS Appl Mater Interfaces 2015;7:26022–35.